RSC Advances

ROYAL SOCIETY OF CHEMISTRY

www.rsc.org/advances

Preparation and pore structure stability at high temperature of silicon-doped ordered mesoporous alumina

Xiaoliang Zhao,[a] Ying Zheng,*[b] Yong Zheng,[c] Yingying Zhan[c] and Xuelin Zheng[b]

Abstract:

Silicon-doped ordered mesoporous aluminas with varying dopant concentration were designed and synthesized in an HCl-acidified sol-gel system with the solvent consisting of ethanol and 2-propanol. When calcined at 800 ℃, all the samples yielded 2-D hexagonal *P6mm* structures. However, for different sample the original periodic structure was retained at a different level upon a high calcination temperature of 1000 ℃. The surface area, pore volume, and mean pore size of the samples with the Si/Al molar ratios ranging from 6% to 11% calcined at 1000 ℃ were determined to be in the range of 235-250 m^2 g^{-1}, 0.60-0.65 cm^3 g^{-1} and 6.8-7.0 nm, respectively. Based on the structural and textural properties characterized by X-ray diffraction (XRD), differential thermal analysis (DTA), N_2 physisorption measurement, transmission electron microscope (TEM) and X-ray photoelectron spectroscopy (XPS), it was speculated that the different degree of the structure-retention is related to the shrinkage caused by the sintering and crystallization of the framework, which was determined by the silicon content in the framework. As compared with other samples, the sample with the Si/Al molar ratio of 11% showed a better structure preservation during the thermal crystallization process, indicating an excellent thermal stability of its pore structure.

Keywords: ordered mesoporous alumina; silicon-doped; thermal stability; sol-gel; preparation

[a]*College of Chemistry and Chemical Engineering, Fujian Normal University, Fuzhou, Fujian 350007, China. Fax: +86 591 83443038; Tel: +86 591 83443038; Email: 1420468290@qq.com*

[b]*College of Materials Science and Engineering, Fujian Normal University, Fuzhou, Fujian 350007, China. Fax: +86 591 83464353; Tel: +86 591 83464353; E-mail: zhn63200@163.com; Zyingth@sina.con*

[c]*College of Chemistry and Chemical Engineering, Fuzhou University, Fuzhou, Fujian 350002, China. Fax: +86 591 83731234-8601; Tel: +86 83731234-8601; E-mail: jennyzan@fzu.edu.cn*

1. Introduction

Ordered mesoporous alumina (OMA) possesses many attractive properties, such as high surface area, large pore volume, narrow pore size distribution (PSD) and unique amphoteric property of γ-phase, which provide it with potential applications in catalysis, adsorption, separation and sensors.[1-4] However, the susceptibility to hydrolysis of the aluminum precursor and phase transition accompanied by the thermal breakdown of the structural integrity makes it difficult to retain the ordered mesostructure at high temperature.[2,5,6] Therefore, it is a challenging task to synthesize OMA with well-defined pores and γ-Al_2O_3 framework at high temperature.[2]

Nanocasting method, with the ordered mesoporous carbon as the template, is one of the methods normally used for synthesizing OMA. By sustaining the local strain caused by the crystallization of the precursor with the rigid carbon template under insert atmosphere and subsequently removing the template by calcination in air, this method is advantageous for preparing the crystalline OMA with well-defined mesostructure.[2] Zhang *et al.*[7,8] synthesized ordered mesoporous γ-Al_2O_3 via a double-replica route, with the carbon material replicated from ordered mesoporous silica (SBA-15 or KIT-6) as the template, by impregnating the carbon matrix with the aluminum precursor at least four times and removing the carbon template at 550 ℃. But when the crystalline temperature was above 750 ℃, the ordered mesostructure was significantly destroyed by the overgrowth of γ-Al_2O_3 nanoparticles and phase transition from γ-phase to δ-phase. Zhao *et al.*[9] yielded ordered mesoporous γ-Al_2O_3 with different mesoporosity by repeating the impregnation procedure two or three cycles and removing of the carbon template prepared from organic-organic self-assembly at 600 ℃. But the ordered mesostructure would deteriorate or collapse after the calcination at 700-900 ℃ for 1 h. Recently, Tiemann *et al.*[10] achieved ordered mesoporous γ-Al_2O_3 in a economical and faster nanocasting method with only one impregnation process by treating the melt aluminum precursor in an ammonia vapor at 60-120 ℃ for 3-7 h and a crystalline temperature of 700 ℃ under N_2 atmosphere. However, δ-Al_2O_3 appeared in the γ-Al_2O_3 framework associated with the undesirable damage of the mesostructure when the crystalline temperature was

900 ℃. Another method normally used for the synthesis of OMA is sol-gel method which adopts surfactant as the template. This method generally includes preparing the aluminum precursor solution and an evaporation-induced self-assembly (EISA) process to form the ordered surfactant-inorganic hybrid before the thermal removal of the template, and the key issue is to control the hydrolysis-condensation behavior of the aluminum precursor.[2] However, the pore structure stability of the final product depends highly on the sol-gel parameters like water and acid concentration,[11-14] as well as the choice of the solvent,[15] surfactant,[3,16,17] swelling agent,[18] carboxylic complexing agents,[12,19] etc. Niesz *et al.*[11] reported the first example of sol-gel synthesized OMA with the triblock copolymer Pluronic P123 ($EO_{20}PO_{70}EO_{20}$, EO = ethylene oxide; PO = propylene oxide) as the template, although the framework was amorphous, by controlling the hydrolysis-condensation rate of the aluminum precursor (aluminum tert-*sec*-butoxide (Al*s*Bu)) with proper content of hydrochloric acid and conducting the EISA process at 40 ℃ under a N_2 flow. Following the procedure introduced by Niesz *et al.*,[11] Pérez *et al.*[15] achieved crystallined sol-gel products with γ-Al_2O_3 framework, well-retained wormhole pore structure and high surface area at 800 ℃ by adopting Al*s*Bu as the aluminum precursor and replacing the ethanol solvent with the *sec*-butanol as well as performing the EISA process at 60-80 ℃, but the structure collapsed when calcined at 900 ℃. Yuan *et al.*[12] introduced a facile and reproducible sol-gel method in which the EISA process was conducted in air and obtained ordered mesoporous γ-Al_2O_3 with high thermal stability up to 1000 ℃ coupled with a big surface area (116 m^2 g^{-1}) by using HNO_3 as the pH adjustor, and this strategy had been widely exploited to synthesis OMA monoliths and OMA-based composite materials,[20-23] which broadened the applicability of sol-gel synthesized OMA. But in the same research,[12] the ordered mesoporous γ-Al_2O_3 synthesized with the pH adjustor of HCl plus carboxylic chelating agents (*e.g.* citric, tartaric and DL-malic acid) which were employed to retard the hydrolysis of aluminum precursor by blocking the reactive sites and protect the assembly-process by chelation, could only thermal stable up to 900 ℃. Li and co-workers[24] recently obtained ordered mesoporous zirconia-alumina material which could maintain the well-ordered

mesostructure and γ-Al_2O_3 framewrok at 1000 ℃ with a surface area of 187 m^2 g^{-1} in the presence of HCl and citric acid. Our group had also prepared OMA supported ceria-zirconia material and lanthanum-doped OMA without transformation from γ- to α-Al_2O_3 at 1000 ℃ in a sol-gel solution consisting of HCl, citric acid and salicylic acid, which exhibit the surface area of 115 m^2 g^{-1} and 205 m^2 g^{-1}, respectively.[25-27] In this report, we try to improve the thermal stability of OMA one step further by doping silicon in the framework, since silicon is considered to be more effective in suppressing the phase transition of γ-Al_2O_3 than rare-earth or alkaline-earth metals.[28] However, the reactivity of aluminum alkoxide is much higher than that of silicon alkoxide which often leads to the undesirable macro-scale phase separation and disrupts the co-assembly process, so the growth kinetics of the silicon and aluminum alkoxide should be controlled and matched to ensure a homogenous precursor.[13,19] Stucky *et al.*[19] synthesized 2-D hexagonal ordered mesoporous amorphous alumina-silica material at 350 ℃ with another triblock copolymer F127 ($EO_{96}PO_{70}EO_{96}$) as the template together with aluminum butoxide and Tetraethylorthosilicate (TEOS) as the inorganic precursors in an ethanolic sol-gel solution acidified by HCl or HNO_3 and with the acetic acid modifying the condensation kinetics of the inorganic alkoxides.[19] Recently, Kosuge *et al.*[5] yielded the silicon-doped mesoporous γ-Al_2O_3 via a simple EISA method by utilizing triblock copolymer as the template combined with AlsBu and TEOS as the inorganic precursors without adding any water and acid when preparing the precursor solution. Although the as-synthesized pore structure did not show obvious pore symmetry, it could maintain the original mesostructure and the uniform pore size at 1000 ℃.

It has been reported that strong aqueous acid such as HCl can partially hydrolyze and charge the inorganic precursor to enhance the affinity for the hydrophilic block of the template which is required for cooperative assembly.[19] With respect to that, the silicon-doped OMA in this work will be synthesized through a sol-gel pathway in the presence of HCl. Meanwhile, we also made some modification to the experimental factors as compared with Yuan's work,[12] such as, controlled addition of hydrochloric acid amount, adding extra 2-propanol (the co-solvent) besides ethanol solvent, a

stepwise EISA process in the absence of carboxylic chelating agents, etc. On the other hand, considering that the excessive silicon can lead to the formation of mullite accompanied with the decrease of the surface area and the destruction of the pore structure,[5,29-31] it is also worthwhile to systematically investigate the relationship between the pore structure stability and silicon content.

2. Experimental

2.1 Synthesis of silicon-doped OMA

In a typical synthesis, a certain amount of Tetraethylorthosilicate (TEOS, Acros, 98%) was dissolved in 4 mL of 2-propanol to form solution A. Meanwhile, approximately 1.00 g of Pluronic P123 (Sigma-Aldrich, M_{av} = 5800) was dissolved in a mixture of 6 mL of ethanol and 1.0 mL of hydrochloric acid (37 wt%) to form solution B. Solution B was added in solution A to form a new solution C, and 4 mL ethanol was used to thoroughly transfer solution B. The solution C was firstly stirred 30 min and then stand quietly for *ca.* 10 h. After that, 0.01 mole of aluminum isopropoxide ($(Al(OiPr)_3)$, Acros, 98+%) was added to solution C under stirring and then the whole mixture should be sealed and vigorously stirred for 10 h. The resulting precursor solution was aged in air at ambient temperature for 24 h to get a wet gel. Then the wet gel was transferred to a drying oven to undergo the solvent evaporation process at 60 ℃ for 10 h and at 80 ℃ for an additional 12 h. Finally, the transparent dried gel (xerogel) was calcined at 1000 ℃ in air for 1h with an intermediate step at 800 ℃ for 1h (5 ℃ min^{-1} ramping rate). In the synthetic system with the pH of ca. 0.85, the content of $Al(OiPr)_3$ was kept constant and the silicon-doped samples were prepared with Si/Al molar ratio in the initial composition (*i.e.*, n(TEOS)/n($Al(OiPr)_3$)) of x : 100, x = 1, 6, 11, 16, 21, 26 and 31. And all the synthesized xerogels were labeled as SA-x% (x = 1, 6, 11, 16, 21, 26 and 31). To better understand the effect of silicon dopant concentration on the textural and structural parameters of OMA, un-doped OMA sample was fabricated via the same strategy for comparison and was labeled as SA-0%.

2.2 Characterization

X-ray diffraction (XRD) patterns were recorded on a Philips X'pert pro MPD

diffractometer with Cu Kα radiation. Differential thermal analysis (DTA) experiments were operated on a Perkin-Elmer 1700 apparatus under air (30 mL min^{-1}) with a heating rate of 5 ℃ min^{-1}. The N_2 physisorption measurements were conducted on a Quantachrome NOVA 4200e Surface Area & Pore Size Analyzer at -196 ℃ after the samples were vacuum-dried at 300 ℃ for 3 h. Surface areas were determined using the Brunauer-Emmett-Teller method. Pore volumes were estimated from the desorption isotherm at a relative pressure of 0.98. Pore diameter distribution (PSD) curves and the mean pore diameters were calculated via the Barrett-Joyner-Halenda theory. Transmission electron microscopy (TEM) images were taken using FEI Tecnai G2 F20 S-TWIN (200 eV) electron microscope attached with an Energy-dispersive X-ray (EDX) spectrometer to detect the chemical components. X-ray Fluorescence (XRF) experiments were carried out on a PANalytical Axios XRF Petro Spectrometer to characterize the content of Si and residual Cl. X-ray photoelectron spectroscopy (XPS) measurement was performed on a Thermo Scientific ESCALAB 250 spectrophotometer using Al-Kα radiation (1486.6 eV) to detect the chemical state of the Si, Al and O and the binding energy (BE) values were calibrated by C 1s peak (284.65 eV).

3. Results and discussion

3.1 Structural and textural properties of silicon-doped OMA

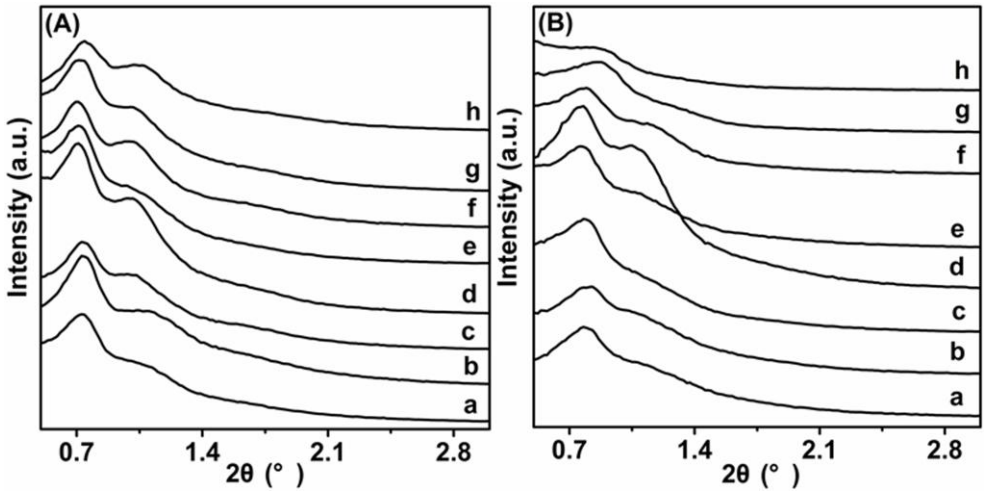

Fig. 1 Small-angle X-ray diffraction (SAXD) patterns for the samples prepared with different Si/Al molar ratios calcined at (A) 800 ℃ and (B) 1000 ℃. a: SA-0%, b: SA-1%; c: SA-6%; d: SA-11%; e: SA-16%; f: SA-21%; g: SA-26%; h: SA-31%.

The small-angle X-ray diffraction (SAXD) patterns of all the samples are used to evaluate the pore symmetry. In Fig. 1A, two well-resolved peaks at *ca.* 0.70 ° and 1.05 ° can be observed in all the profiles indicating the samples calcined at 800 ℃ possess similar pore structure. According to the previous study,[32] this structure can be attributed to the 2-D hexagonal symmetry with *P*6*mm* space group and the aforementioned two peaks can be indexed as the (10) and (11) reflections, respectively. But the SAXD patterns for samples calcined at 1000 ℃ (Fig. 1B) are different from each other, which suggests that the original similar ordered pore structures are differently retained among these samples. The gradual increase in the intensity of (10) peak in the following sequence of SA-0%, SA-1%, SA-6% and SA-11% at 1000 ℃ indicates the direction of gradual enhancement of the pore structure, whereas the (10) peaks of SA-16%, SA-21%, SA-26% and SA-31% are found to decrease their intensities with increasing the silicon content which reveals the gradual deterioration of their mesostructure.[33] Further observation shows that the related (10) and (11) peaks of each samples calcined at 1000 ℃ (Fig. 1B) appear with low-intensity and shift to higher angle position as compared to their counterparts at 800 ℃ (Fig. 1A) indicating the structural deterioration and shrinkage which may be caused by the crystallization of the precursor occurred in the frameworks.[8,18,21,32]

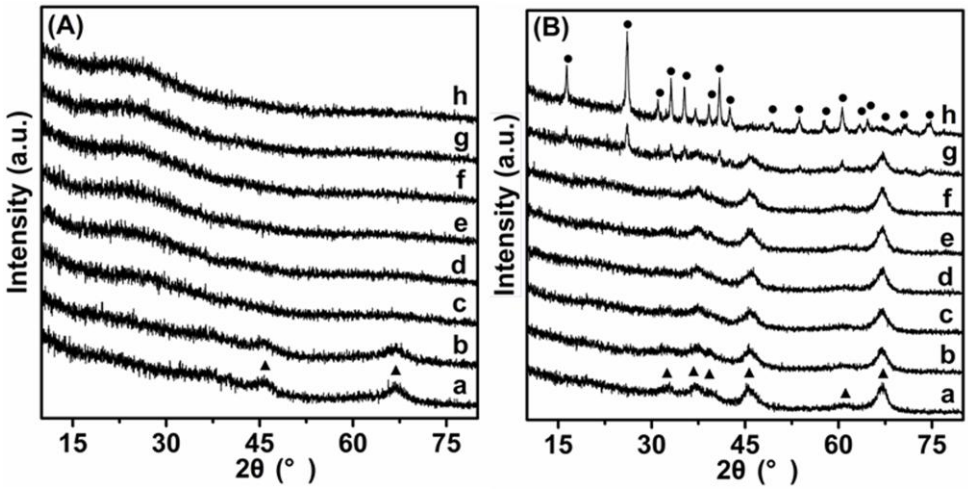

Fig. 2 Wide-angle X-ray diffraction (WAXD) patterns for the samples prepared with different Si/Al molar ratios calcined at (A) 800 ℃ and (B) 1000 ℃. a: SA-0%, b: SA-1%; c: SA-6%; d: SA-11%; e: SA-16%; f: SA-21%; g: SA-26%; h: SA-31%. (▲) γ-Al_2O_3; (●) mullite.

As justified by the wide-angle X-ray diffraction (WXRD) patterns given in Fig. 2A, SA-0% displays two broad and diffuse peaks at around 45.5 °and 67.0 °which can be indexed as (400) and (440) reflections of γ-Al_2O_3 (JCPDS 10-0425).[8,10,34,35] SA-1% also shows a similar pattern but the related peak intensities indicate that the crystalline degree of γ-Al_2O_3 is somewhat lower than that of SA-0%, while other silicon-doped samples (SA-x% ($x \geq 6$)) are amorphous as no discernable peaks can be detected in their WAXD profiles. The less crystalline of the silicon-doped samples compared with un-doped sample (SA-0%) may explain their higher structural order reflected by the apparent SAXD patterns (Fig. 1A).[15] But as deduced by the WXRD patterns of the samples calcined at 1000 ℃ in Fig. 2B, SA-0% presents more crystallized γ-Al_2O_3,[15,20,36] Meanwhile, the silicon-doped samples also show high degree of crystallinity as evidenced by the relevant noticeable WXRD patterns: the phase of SA-x% ($1 \leq x \leq 21$) can be indexed as either γ-Al_2O_3 or spinel as these two phase are very hard to distinguish by normal X-ray diffraction,[31] and the phase of SA-31% can be attributed to mullite,[29,31] but the crystalline phase of SA-26% is a little complicated because some peaks characteristic of mullite are also visible besides those similar to SA-x% ($1 \leq x \leq 21$).

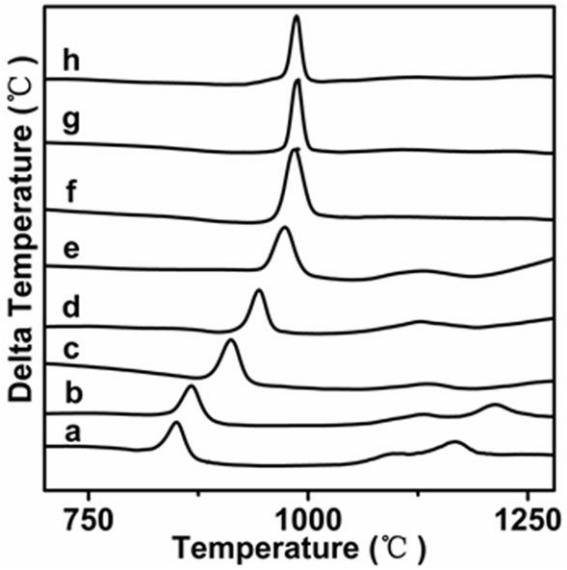

Fig. 3 DTA curves for the samples prepared with different Si/Al molar ratios 720-1290 ℃. a: SA-0%, b: SA-1%; c: SA-6%; d: SA-11%; e: SA-16%; f: SA-21%; g: SA-26%; h: SA-31%.

To estimate the crystallization temperature and the thermal stability of these samples, DTA measurements were performed. As can be seen from the DTA curves in Fig. 3, SA-0% shows three exothermic peaks positioned at *ca.* 840 ℃, 1090 ℃ and 1170 ℃ which can be assigned to the crystallization of γ-Al_2O_3 and its subsequent transformation to intermediate phase (*e.g.* δ or θ-Al_2O_3) and α-Al_2O_3, respectively. SA-1% also shows three peaks locating at *ca.* 870 ℃, 1130 ℃ and 1213 ℃ respectively which suggests that the crystallization and transformation temperature of γ-Al_2O_3 can be improved by doping even a small amount of silicon into the alumina host.[29] On the other hand, the crystallization temperature from amorphous state for SA-x% ($1 \leq x \leq 21$) samples is positively correlated with the silicon content (*ca.* 870 ℃ for SA-1%, *ca.* 912 ℃ for SA-6%, *ca.* 942 ℃ for SA-11%, *ca.* 973 ℃ for SA-16% and *ca.* 980 ℃ for SA-21%) while that of SA-x% ($21 \leq x \leq 31$) keeps unchanged. However, SA-x% ($1 \leq x \leq 16$) display a second peak representing phase-transformation temperature at *ca.* 1130 ℃ while SA-x% ($21 \leq x \leq 31$) do not show other DTA peaks except the one at *ca.* 980 ℃. This suggests that the samples with different silicon dopant concentrations have different crystallization process and the crystallizations of all the samples are almost complete at 1000 ℃. Connecting to the result of Fig. 2B, it is very likely that the crystal phases of SA-x% ($1 \leq x \leq 16$) are γ-Al_2O_3, SA-21% is spinel which crystallizes from the γ-Al_2O_3 structure,[37] SA-26% is a mixture of spinel and mullite, and SA-31% is single mullite phase.

Fig. 4 gives the N_2 adsorption-desorption isotherms and PSD curves of all the samples. Fig. 4A and B show that all the samples display Ⅳ-type isotherms with H1-type hydrolysis loops which indicates the existence of cylindrical mesopores in all the samples at both 800 ℃ and 1000 ℃.[14,20-23] However, a shift in the capillary condensation steps towards higher relative pressure with the calcination temperature increasing from 800 ℃ to 1000 ℃ also indicates the increase in the pore size among these samples.[14,17,21,33] In Fig. 4C, both SA-0% and SA-1% present a broad peak centered at *ca.* 8.8 nm while SA-x% ($6 \leq x \leq 31$) show a narrow peak with the maximum at *ca.* 7.0 nm, at the same time, small mesopores with the size centered at *ca.* 3.3 nm increase with the increase of the Si/Al molar ratio in the initial

composition. And these small mesopores (*ca.* 3.3 nm) also result in obvious delay in the desorption branches of SA-16%, SA-21%, SA-26% and SA-31% which suggests there are condensation and partial blocking in the pores of these samples.[17] It is anticipated that these small pores (*ca.* 3.3 nm) come from the decomposition of poly (ethylene oxide) (PEO) blocks of P123 and should interpenetrate into the framework.[33] Because in the experiment, the TEOS is added in the synthetic system prior to Al(O*i*Pr)$_3$ owing to the dissimilar hydrolysis-condensation kinetics and chemistry of the aluminum and silicon alkoxide.[33,38] The pre-hydrolysized TEOS can interact preferentially with the PEO blocks, and for this reason the silicon species will

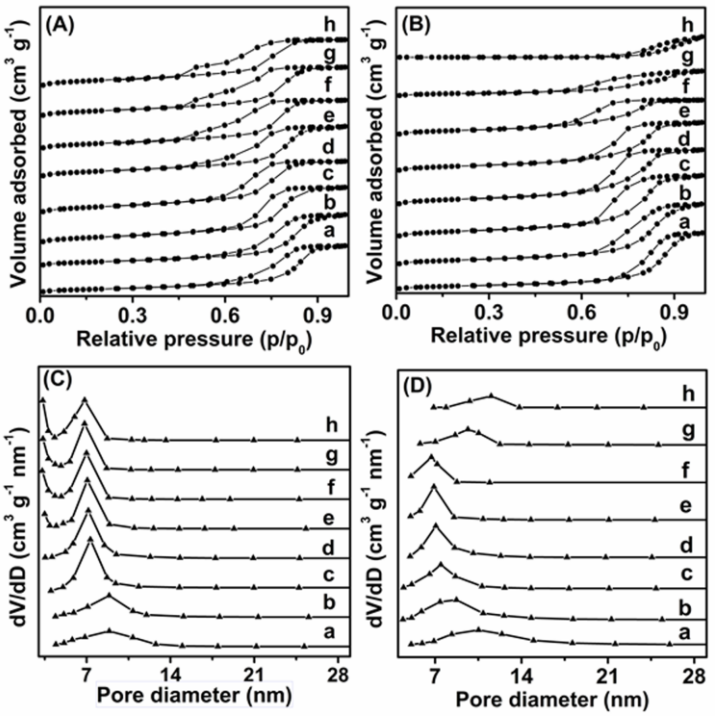

Fig. 4 N_2 adsorption-desorption isotherms and PSD curves for the samples prepared with different Si/Al molar ratios calcined at (A, C) 800 ℃ and (B, D) 1000 ℃. a: SA-0%, b: SA-1%; c: SA-6%; d: SA-11%; e: SA-16%; f: SA-21%; g: SA-26%; h: SA-31%.

stay at the surface of the pores coming from the removal of the PEO blocks, meanwhile the surface hydroxyls and activated atomic diffusion in the surface sites and bulk sites can be reduced by the Si atoms leading to a suppression of the crystallization, grain growth, phase transition and sintering processes in these places,[28-30,39] so the small mesopores can be stabilized and the number of them will

increase with raising the silicon content. But those small pores (*ca.* 3.3 nm) disappear at 1000 ℃ and all the samples show a unimodal peak in their PSD curves (see at Fig. 4D) which may be correlated to the crystallization of the precursor and sintering of the crystalline particles at elevated temperature.[35] On the other hand, as indicated by the shift in the capillary condensation steps, the increase in the pore size with the calcination increasing from 800 ℃ to 1000 ℃ can also be confirmed by the PSD peaks in Fig. 4C and D, in particular, SA-0%, SA-26% and SA-31% exhibit remarkable shift of the peak position (*ca.* 8.9 nm to *ca.* 10.5 nm for SA-0%, *ca.* 6.8 nm to *ca.* 9.7 nm for SA-26% and *ca.* 6.7 nm to *ca.* 11.2 nm for SA-31%), which reveals the structural collapse of these samples caused by the crystallization and sintering under the condition of lacking or excessive silicon, respectively.

Table 1 Textural parameters of the samples prepared with different Si/Al molar ratios calcined at different temperatures

	800 ℃			1000 ℃		
Sample	S_{BET}/m^2 g^{-1}[a]	V_p/cm^3 g^{-1}[b]	D_p/nm[c]	S_{BET}/m^2 g^{-1}[a]	V_p/cm^3 g^{-1}[b]	D_p/nm[c]
SA-0%	212	0.66	7.5	136	0.51	11.6
SA-1%	247	0.73	7.5	180	0.56	8.6
SA-6%	343	0.76	6.7	250	0.65	7.0
SA-11%	361	0.77	6.5	235	0.60	6.9
SA-16%	323	0.73	5.9	170	0.45	6.5
SA-21%	315	0.72	4.9	158	0.33	5.1
SA-26%	318	0.70	4.8	115	0.25	10.3
SA-31%	339	0.69	4.5	22	0.12	11.8

[a]BET surface area, [b]pore Volume and [c]mean pore size of the samples deprived from the physisorpitons measurements.

Table 1 summarizes the textural properties of the samples calcined at different temperatures. For the samples calcined at 800 ℃, the surface area and pore volume continuously increase with increasing the silicon content and reach the maximum at SA-11% followed by gradual slowdown of the increase tendency. An analogous

phenomenon is also observed in the samples calcined at 1000 ℃ but the maximum appears at SA-6%. It is worthy to note that SA-6% show higher surface area and pore volume than SA-11% at 1000 ℃ (250 m^2 g^{-1} *vs.* 235 m^2 g^{-1}, 6.7 cm^3 g^{-1} *vs.* 6.5 cm^3 g^{-1}) despite the fact that its mesoscopic order is lower than that of SA-11% as supported by the intensity of the relevant (10) reflections in Fig. 1B. However, since having highly ordered mesostucture is not a prerequisite to obtain a higher surface area,[15] so

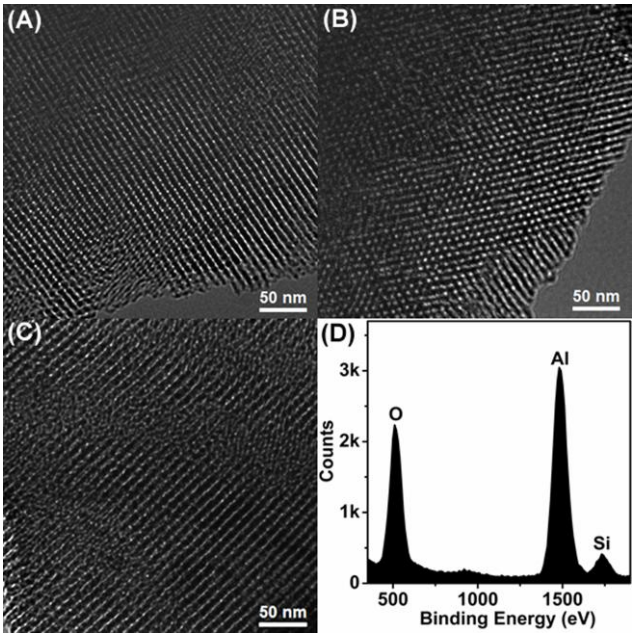

Fig. 5 TEM images of SA-11% calcined at 800 ℃ viewed along (a) [110] and (b) [001] orientations, (c) TEM images and (d) EDS spectrum of SA-11% calcined at 1000 ℃.

the higher surface area of SA-6% in comparison to SA-11% may be due to its smaller pores, which is possibly related to the structural shrinkage during the calcination process,[15] as its PSD maximum (*ca.* 7.4 nm in Figure 4D) at 1000 ℃ is a little larger than its mean pore size (7.0 nm in Table 1).[34] Similarly, SA-16% and SA-21% also show the higher PSD maxima than their mean pore sizes at 1000 ℃ which also are indicative of the existence of small pores, but the reason can be attributed to the pore blocking (SA-16%) or the spinel formation (SA-21%) resulting from the excessive silicon. On the contrary, the PSD maxima of SA-0%, SA-1%, SA-26 and SA-31% are lower than their mean pore sizes (11.2 nm *vs.* 11.6 nm for SA-0%, 8.2 nm *vs.* 8.6 nm for SA-1%, 9.7 nm *vs.* 10.3 nm for SA-26% and 11.2 *vs.* 11.8 nm for SA-31%)

suggesting that the existence of large pores which comes from the collapse of the pore structures resulting from the grain growth or the formation of mullite.[21,31] Compared to other samples in this research, SA-11% shows a PSD maximum (*ca.* 7.0 nm) similar to its mean pore size (6.9 nm) at 1000 ^{o}C, as well as the steep hysteresis loops both at 800 ℃ and 1000 ℃ (Fig. 4 A and B). And more importantly, the calcination at 1000 ℃ don't cause the absence of (11) reflection and significant reduction of the surface area and pore volume, which indicates a high thermal stability of its pore structure.

Fig. 5 A-C provide the TEM images of SA-11% at different temperatures. As can be seen in Fig. 5, parallel channels along [110] orientation (Fig. 5A) and hexagonally packed cylindrical pores along [001] orientation (Fig. 5B) signify the typical 2-D hexagonal mesostructure of SA-11% calcined at 800 ℃. And this mesoscopic regularity can also be well inherited even calcined at 1000 ℃ although accompanied by some small degree of sintering and pore-collapse (Fig. 5C). The result evidences the well-defined structural features of SA-11% at 800 ℃ and 1000 ℃ which matches well with the conclusions drawn from Fig. 1 and 4. Furthermore, the EDX spectrum of SA-11% calcined at 1000 ℃ (Fig. 5D) confirms the presence of O, Al and Si, and the elemental analysis determined from the EDX indicates that the Si/Al molar ratio is 11.3% which agrees well with the theoretic value in the initial composition (11%).

3.2 Effect of 2-propanol, hydrochloric acid and silicon content on the pore structure stability of OMA

As reported by Kosuge *et al.*,[5] the α-Al_2O_3 appears in the un-doped sample and the mullite phase appears in silicon-doped alumina with the Si/Al molar ratio of *ca.* 16% accompanied by the collapse of the pore structure when calcined at 1000 ℃. In contrast, this study shows a different result: both SA-0% and SA-16% can keep the ordered structure and γ-Al_2O_3 phase (see at Fig. 1B and 2B). This result may indicate that the ordered pore-structure can restrain the γ-α phase transition which coincides with the previous statement.[27] Thus, the use of 2-propanol and hydrochloric acid in this study is thought to play an important role in improving the stability of the pore structure of OMA.

3.2.1 Effect of 2-propanol content on the pore structure stability of OMA

As found in the experiment, the shrinkage of the gel which is often encounted in the EISA process can be reduced by adding some 2-propanol. But if the 2-propanol content exceeds 8 mL, unideal xerogel with uneven surface or visible crack will be gained indicating that large amount of 2-propanol may destroy the sol-gel process of the alumina. To elucidate the effect of 2-propanol content on the pore structure stability of OMA in some detail, we conduct some additional experiments according to the procedure described in section 2.1 without adding TEOS. The total volume of the solvent keeps constant (*ca.* 14 mL) while the volume of ethanol or 2-propanol vary, and the resultant samples are donated as SA(mY)-0% (where m is the volume of the 2-propanol). As an example, the sample synthesized with 4 mL 2-propanol can be donated as SA(4Y)-0%, *i.e.* SA-0%.

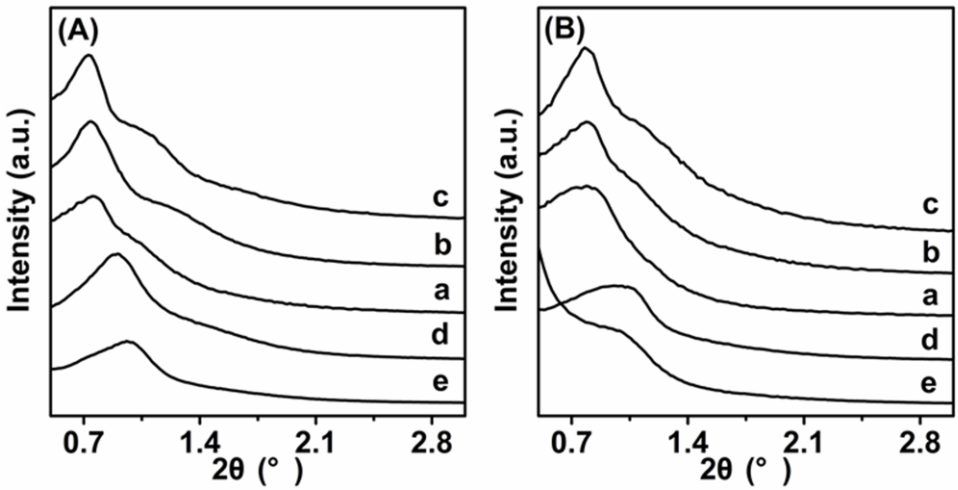

Fig. 6 The SAXD patterns for the samples prepared with different 2-propanol content calcined at (A) 800 ℃ and (B) 1000 ℃. a: SA(0Y)-0%; b: SA(2Y)-0%; c: SA(4Y)-0%; d: SA(6Y)-0%; e: SA(8Y)-0%.

Displayed in Fig. 6 are the SAXD patterns of these samples at different temperatures. As can be seen in Fig.6 A, the sample synthesized with the solvent of ethanol (SA(0Y)-0%) shows a apparent peak at *ca.* 0.70 ° and a small peak at 1.05 ° indicating that its pore structure is similar to SA-0%, but a significant decrease in the peak intensity occurs upon calcination at 1000 ℃ (Fig. 6B) indicating the less stability of its pore structure compared with that of SA-0%. On the other hand, with the content of 2-propanol increasing to 2 mL and 4 mL, the diffractions at both *ca.*

0.70 ° and 1.05 ° become more pronounced at both 800 ℃ and 1000 ℃ (see at Fig. 6A and B) which suggests the development of the pore structure stability.[33] But for the two samples synthesized with 6 mL and 8 mL 2-propanol (*i.e.*, SA(6Y)-0% and SA(8Y)-0%), only one single peak at *ca.* 0.9 ° appears in their patterns when they are calcined at 800 ℃ (see at Fig.6A), which indicates some reorganization of the pore structures, and the SAXD profiles in Fig. 6B also indicates that their pore structure don't show good stability against high-temperature, particularly in the case of SA(8Y)-0% no discernable peak can be detected indicating a significant deterioration of its pore structure. The result above may discloses the effect of the 2-propanol on the pore structure to some extent: (ⅰ) proper content of 2-propanol can improve the ordering and stability of pore structure by controlling the hydrolysis-condensation rate of the aluminum precursor. According to the sol-gel chemistry,[40] the hydrolysis and condensation of aluminum alkoxide will produce 2-propanol. In addition, the ligand exchange reaction between ethanol and Al(O*i*Pr)$_3$ will also release 2-propanol besides Al-triethoxide which can accelerate the hydrolysis rate as well and lead to a highly polymerized aluminum species.[15,18] So the addition of 2-propanol may shift the chemical equilibriums of the above reactions (hydrolysis, condensation and ethanol exchange reactions) to the reactant side, and thus control the sol-gel process of alumina which is a key issue to obtain the well-defined pore structure because low degree of oligomerization is helpful to assemble well around the block copolymer to form a better mesophase.[2,12] (ⅱ) The large amount of 2-propanol may lead to a transition of the pore structure and reduce its stability which may be due to that the condensation of aluminum species is seriously interfered and therefore results in a poly-organized surfactant-inorganic hybrid.[15]

3.2.2 Effect of hydrochloric acid content on the pore structure stability of OMA

Hydrochloric acid serves an important factor which affects the final pore structure because the hydrochloric acid not only act as the catalyst (HCl) but also provide the necessary water for the hydrolysis of aluminum precursor. In the previous study of Yuan *et al.*, when adopting 1.4-1.6 mL hydrochloric acid (37 wt%) as the pH adjustor, the long-range ordered pore structure cannot be yielded. Additionally, in this

study it was found experimentally that if hydrochloric acid was used less than 1.0 mL, $Al(OiPr)_3$ could not be well dissolved or the xerogel formed quickly which may be attributed to the low water and acid content.[11,12] To explore the effect of hydrochloride acid content on the pore structure stability of the final product, we prepared three samples with the same manner as SA-0% but increase the hydrochloride acid content to 1.2, 1.4 and 1.6 mL, and as-synthesized samples are donated as SA(1.2H)-0%, SA(1.4H)-0% and SA(1.6H)-0%, respectively.

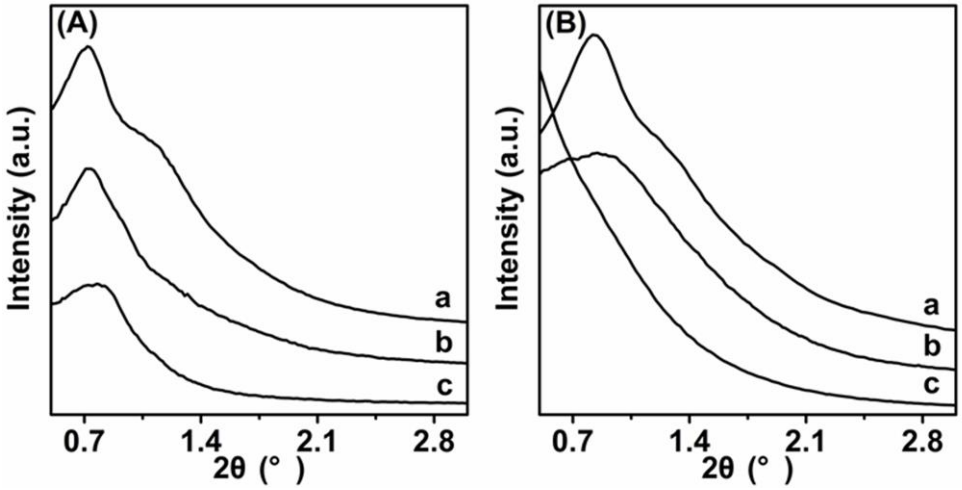

Fig. 7 The SAXD patterns for the samples prepared with different hydrochloric acid content calcined at (A) 800 ℃ and (B) 1000 ℃. a: SA(1.2H)-0%; b: SA(1.4H)-0%; c: SA(1.6H)-0%.

Fig. 7 shows the SAXD patterns of the samples calcined at different temperatures. As justified by the SAXD patterns in Fig.7 A, all the three samples should possess hexagonally ordered pore structure, but the structural order decreases with increasing the hydrochloric acid content. And after calcination of 1000 ℃, as shown in Fig.7 B, only SA(1.2H)-0% keep the intense SAXD peak suggesting the excellent stability of its pore structure, meanwhile, the weak and broad peak suggests the reduction of the mesoscopic ordering in SA(1.4H)-0% although the structural ordering is partly preserved,[33] but for SA(1.6H)-0% the discernable SAXD peak can hardly be identified suggesting the absence of the ordered pore structure. The result above reveals the strong influence of hydrochloric acid content on the pore structure stability. However, it's necessary to examine the effect of water content and HCl content on the pore structure stability respectively to obscure a comprehensive

understanding of the influence of hydrochloric acid. Considering that the molar ratio of water to aluminium precursor in the initial composition (donated as $n(H_2O)/n(Al(OiPr)_3)$) values in 1.2 mL, 1.4mL and 1.6 mL hydrochloric acid are 4.9, 5.8 and 6.6 respectively, three reference samples are also prepared by increasing the $n(H_2O)/n(Al(OiPr)_3)$ values of SA-0% to 4.9, 5.8 and 6.6 with purified water and the as-prepared samples are donated as SA(tW)-0% (t stands for the $n(H_2O)/n(Al(OiPr)_3)$ values and t = 4.9, 5.8 and 6.6).

Fig. 8 presents the SAXD patterns of the samples at different temperatures. It should be noticed that all the three sample exhibit noticeable typical 2-D hexagonal SAXD patterns both at 800 ℃ and 1000 ℃, and no significant decrease of the intensity of the diffraction line appears during the calcination between 800 and 1000 ℃ indicating a high temperature stability of their pore structures.

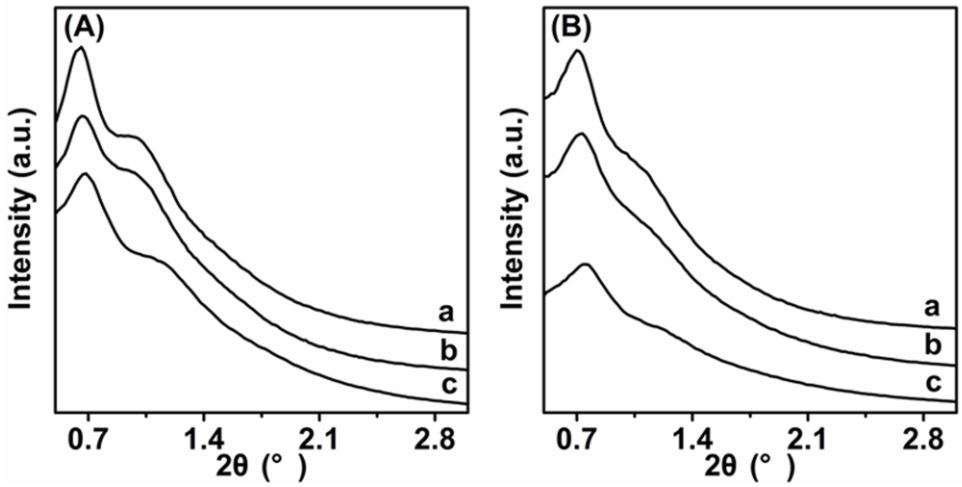

Fig. 8 The SAXD patterns for the samples prepared with different $n(H_2O)/n(Al(OiPr)_3)$ values calcined at (A) 800 ℃ and 1000 ℃. a: SA(4.9W)-0%; b: SA(5.8W)-0%; c: SA(6.6W)-0%.

On the other hand, a little decrease of the peak-intensity with $n(H_2O)/n(Al(OiPr)_3)$ values increasing can also be observed indicating that increase of water content can also reduces the ordering of the pore structure to some degree. According to the proceeding report,[40] the negative charge of O atoms in water will attack the electropositive Al atoms in Al(O*i*Pr) and produces Al-OH groups in the hydrolysis step, and the condensation and polymerization of the Al-OH and Al-OR (RO- refers to alkoxy ligand) groups creates Al-O-Al bonds and Al oligomers. So it's likely that the

increase of water content will increase the number of Al-OH groups and Al oligomers which may account for the decrease of the mesoscopic order in SA(4.9W)-0%, SA(5.8W)-0% and SA(6.6W)-0%, as explained before. Therefore, the reason why the highly thermal stable ordered pore structure can be gained with 1.4-1.6 mL hydrochloric acid (37 wt%) as the pH adjustor as that of 1.4-1.6mL nitric aicd (67 wt%), as reported in Yuan's study, may partly related to the difference in water content (the $n(H_2O)/n(Al(OiPr)_3)$ values for the former is *ca.* 5.8-6.6 while that for the later is *ca.* 3.6-4.1).

Now that SA-0%(6.6W) can preserve its mesoscopic order up to 1000 ℃, so the major factor responsible for the loss of structural order in SA(1.6H)-0% may be correlated to the increase of H^+ and Cl^- content. It has been suggested that the H^+ in the system will strengthen the interaction inorganic precursors and the organic template which allows a symmetric growth of inorganic oligomers in the hydrophilic domains and finally results in the formation of well-organized inorganic-organic hybrids.[36] Thus, it is assumed that in Kosuge's study the interaction between the inorganic precursors and the organic template is weak coordination bonds, while that in this study is stronger hydrogen bonds which contribute to the higher pore structure ordering. But on the other hand, large content of H^+ will also proton the Al-OH groups to form $Al\text{-}OH^+$ which is no longer hypocritical and thus slows down the condensation reactions of the aluminum precursor which also hinders the self-assembly process.[15,40]

As for the function of Cl^- on pore structure stability, Yuan *et al.*[12] proposed that the Cl^- will coordinate strongly to the Al^{3+} to destroy the balance of the organic-inorganic interface and disturb the self-assembly process which leads to the loss of long-range ordered structure. As listed in Table 2, the content of residual Cl in SA-0% is 0.11 wt% at 800 ^oC and 0.05 wt% at 1000 ^oC suggesting that the calcination contributes to the elimination of redisual Cl. In addition, SA(1.6H)-0% shows higher residual Cl content than SA-0% both at 800 ^oC (*ca.* 0.15 wt%) and 1000 ^oC (*ca.* 0.08 wt%). But in SA(6.6W)-0%, the content of residual Cl is similar to that SA-0% at 800 ^oC while a little larger as compared to SA-0% at 1000 ^oC (*ca.* 0.06 wt%) suggesting

that the increase of water content hinders the elimination of residual Cl between 800 and 1000 ^{o}C which can also explain the deterioration in the pore structure of SA(6.6W)-0% and SA(1.6H)-0% (see at Fig. 7 and 8). It seems that the high content of residual Cl in SA(1.6H)-0% not only disturbs the self-assembly process but also reduces the stability of the pore structure resulting in a pore structure with low order and thermalstability (see at Fig. 7). On the other hand, it can be seen from Table 2 that the increase of silicon content reduces residual Cl content significantly: with the Si/Al

Table 2 The content of the silicon and the residual chloride in the samples calcined at different temperatures

Sample	Initial composition[a]	Si(wt%)		Cl(wt%)	
	HCl/H_2O/TEOS/Al(O*i*Pr)$_3$	800^{o}C	1000^{o}C	800^{o}C	1000^{o}C
SA-0%	1.2/4.1/0/1	—	—	0.11	0.05
SA(1.6H)-0%	1.9/4.1/0/1	—	—	0.15	0.08
SA(6.6W)-0%	1.2/4.9/0/1	—	—	0.11	0.06
SA-1%	1.2/4.1/0.01/1	0.37	0.35	0.07	0.03
SA-6%	1.2/4.1/0.06/1	2.28	2.24	0.04	0.02
SA-11%	1.2/4.1/0.11/1	3.97	4.04	0.02	0.01

[a]The content of the initial composition is expressed in molar ratio terms.

molar ratio in the initial composition increasing from 0 to 0.11, the Cl content decreases from 0.11 wt% to 0.02 wt% at 800 ^{o}C and from 0.05 wt% to 0.01 wt% at 1000 ^{o}C. According to the SAXD analysis in Fig. 1, the structural order will gradually increase with the Si/Al molar ratio increaseing from 0 to 0.11, which may related to the gradual decrease of the residual Cl as present in Table 2. This result also shows the value of introducing silicon in the framework of OMA to improve the stability of the pore structure through reducing the residual Cl level.

3.2.3 Effect of silicon content on the pore structure stability of OMA

On the basis of above analysis, it is easy to understand the effect of the silicon content on the pore structure stability of OMA. For the silicon-doped samples, the co-condensation of Al-OH and Si-OH groups will give up to Al-O-Si linkages

together with Si-O-Si and Al-O-Al linkages.[41] But with the sol-gel technology and confinement effect of the ordered pore structure,[42] a promising dispersion property of the precursor solution can also be achieved, and the evidence can be obtained from the formation of mullite in SA-31% at *ca.* 980 ℃ which indicates that a high homogeneity of the Al and Si atoms in the precursor.[22,38] But if the silicon content is too low to link homogenously with all the Al atoms, the Al-O-Al linkages can still exist. On the other hand, it's well know that the microphase separation of P123 forms a liquid-crystal phase in the presence of inorganic species with a hydrophobic cores containing the cylindrically assembled poly (propylene oxide) (PPO) blocks, and a hydrophilic corona consisting primarily of the PEO blocks,[2,18,32] When P123 self-assembles in the EISA process the inorganic precursors are attached into the hydrophilic segments,[1,2] and when the P123 is removed by the consequent calcination two sets of meospores can be formed: the pores originating from the PPO blocks will be arranged in hexagonal arrays while the pores originating from the PEO chains will stretch in the framework.[32] In view of the prehydrolysis of TEOS, the Si-OH groups will coordinate with PEO chains in advance, so the pores originating from the PEO chains will have a "surface layer" of Si-O-Al linkages where the Si and Al atom are homogenously distributed and a bulk with the most portion is Al-O-Al linkages. And this "heterogenerty" may be confirmed by the segregation of diplustic phase of spinel and γ-Al_2O_3 in SA-26%. But with the calcination at elevated temperature, the Si atoms will migrate from the "surface layer" to the bulk leading to a higher dispersion of Si atoms throughout the alumina framework. And simultaneously, with the crystallization of γ-Al_2O_3 at elevated temperature, the Si atoms will incorporate in the lattice of γ-Al_2O_3.[30]

As we know, the γ-Al_2O_3 has a spinel-like structure with Al^{3+} defects preferably positioned at tetrahedral (*Td*) sites and many vacancies positioned at octahedral (*Oh*) sites.[6,30,34,39] However, according to the previous reports,[29,30] with the incorporation of the Si atoms in the *Td* sites extra Al atoms may be moved from *Td* to *Oh* sites which can decrease the total number of defects and vacancies. Horiuchi *et al.*[30] reported that the silicon content with Si atoms filling all the *Td* sites and Al atoms filling all the *Oh*

sites is 13wt% which is close to the silicon content of SA-11%. Accordingly, SA-11% should have a good dispersion of the Si atoms in the alumina matrix at 1000 ℃. Fig. 9

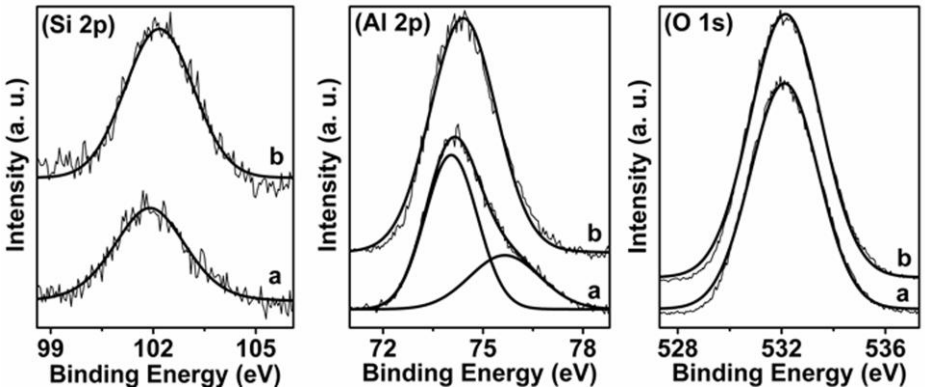

Fig. 9 XPS spectra of Si 2p, Al 2p and O 1s in SA-11% at (a) 800 ℃ and (b) 1000 ℃.

shows the XPS spectra of Si 2p, Al 2p and O 1s in SA-11% at different temperatures. The Si 2p spectra are symmetrical at both 800 ℃ and 1000 ℃ indicating that the coordination state of Si atoms is both homogenous at these temperatures.[29] In addition, the binding energies of Si 2p at 800 ℃ (101.9 eV) and 1000 ℃ (102.2 eV) are both lower than that for pure SiO_2 (104.4 eV),[43] which gives an hint that the Si atoms in the Si-O-Si linkages are substituted by the Al atoms, *i.e.*, an incorporation of Si atoms into alumina matrix.[29] On the other hand, the Al 2p spectrum of SA-11% calcined at 800 ℃ is not symmetrical and can be fitted by two symmetrical Gaussian simulation peaks (positioned at 74.0 eV and 75.6 eV) which corresponding to the two chemical state of the aluminum atoms. And it is reasonable that the Al 2p peak centered at 74.0 eV can be attributed to the Al-O-Al linkages residing in the bulk while the other one centered at 75.6 eV is assigned to the Al-O-Si linkages staying in the "surface layer". But in SA-11% calcined at 1000 ℃, the symmetric Al 2p peak appears besides a symmetric Si 2p peak indicating that the Si and Al atoms are well-dispersed. Meanwhile, the Al 2p peak binding energy (74.4 eV) of SA-11% at 1000 ℃ is higher than that of pure γ-Al_2O_3 (74.2 eV),[44] which further certifies that the formation of Si-O-Al bonds.[45] On the other hand, the binding energies of O 1s of SA-11% at 800 ℃ (532.1 eV) and 1000 ℃ (532.2 eV) lying between that of pure γ-Al_2O_3 (531.5 eV)[44] and pure SiO_2 (533.3 eV)[43] is also a sign that the silicon has enter into the lattice of γ-Al_2O_3.[46] Based on the above analysis, one can speculate that the incorportation of

Si atoms in SA-11% reduces the number of the defects and vacnacies which may stablize γ-Al_2O_3 structure and build a stronge framework to resist the shrinkage of the pore structure during the thermal crystalline process,[30,47] and offers a good structure preservation. And we may then assume that with the initially increase of the silicon content in the case of SA-x% ($0 \leq x \leq 11$), the higher the silicon content is, the lower the defect number is, the less shrinkage the pore structure experiences and the higher the pore structure stability shows. But if the silcion content of the samples is continuously increased, besides the Si atoms occuping the *Td* sites, the extra ones will be isolated as Si-rich microdomains or amporphous silica which can block the pore channels,[5,37,48] as pointed out before. On the other hand, with the migration of the Si atoms from the "surface layer" to the bulk at high temperature the hex-coordinaeted Al atoms increase as well which can lead to the formation of spinel,[48] and the spinel will also react with the amorphous silica or Si-rich domains coming from the extra Si atoms to form mullite which may forms in the surface section (SA-26%) or the whole matrix (SA-31%), both of which can lead to the breakdown of the pore channels and drastic decrease of the textural properties,[31] as demonstrated by the related SAXD patterns in Fig. 1 and the related data in Table 1.

4. Conclusions

In summary, we have reported the preparation of ordered mesoporous γ-Al_2O_3 with high thermal stability up to 1000 ℃ via a sol-gel method by controlling the hydrolysis-condensation of aluminum precursor with HCl and 2-propanol and by substituting aluminum with silicon in tetrahedral position of the crystal structure. The obtained materials are expected to act as eligible candidates for catalysis and adsorption application at high-temperature. Meanwhile, the findings in the present study provide a new opportunity for understanding the synthesis of OMA via a sol-gel process and the structural stability of silicon-doped OMA. We believe this established approach can be extended to the preparation of the highly thermal stable ordered multicomponent mesostructured metal oxides.

Acknowledgements

We greatly thank the financial support from The National Natural Science

Foundation of China (51103025) and Joint Research Program of Fuzhou University (NO: DH-700). This work is also supported by the opening laboratory of Research Institute of Photocatalysis, State Key Laboratory of Photocatalysis on Energy and Environment, Fuzhou University, China.

References

1 K. Ariga, A. Vinu, Y. Yamauchi, Q. Ji and J. P. Hill, *Bull. Chem. Soc. Jpn.*, 2012, **85**, 1.

2 D. Gu and F. Schüth, *Chem. Soc. Rev.*, 2013, Doi: 10.1039/c3cs60155b.

3 W. Cai, J. Yu and M. Jaroniec, *J. Mater. Chem.*, 2011, **21**, 9066.

4 C. Márquez‐Alvarez, N. Žilková, J. Pérez‐Pariente and J. Čejka, *Catal. Rev.*, 2008, **50**, 222.

5 K. Kosuge and A. Ogata, *Microporous Mesoporous Mater.*, 2010, **135**, 60.

6 T. J. Pinnavaia, Z. Zhang and R. W. Hicks, *Stud. Surf. Sci. Catal.*, 2005, **156**, 1.

7 Q. Liu, A. Wang, X. Wang and T. Zhang, *Chem. Mater.*, 2006, **18**, 5153.

8 Q. Liu, A. Wang, J. Xu, Y. Zhang, X. Wang and T. Zhang, *Microporous Mesoporous Mater.*, 2008, **116**, 461.

9 Z. Wu, Q. Li, D. Feng, P. A. Webley and D. Zhao, *J. Am. Chem. Soc.*, 2010, **132**, 12042.

10 S. Haffer, C. Weinberger and M. Tiemann, *Eur. J. Inor. Chem.*, 2012, 3283.

11 K. Niesz, P. Yang and G. A. Somorjai, *Chem. Commun.*, 2005, 1986.

12 Q. Yuan, A. X. Yin, C. Luo, L. D. Sun, Y. W. Zhang, W. T. Duan, H. C. Liu and C. H. Yan, *J. Am. Chem. Soc.*, 2008, **130**, 3465.

13 S. M. Grant and M. Jaroniec, *J. Mater. Chem.*, 2012, **22**, 86.

14 K. L. Martena, S. M. Grant and M. Jaroniec, *ACS appl. Mater. interfaces*, 2012, **4**, 3738.

15 L. L. Pérez, S. Perdriau, G. t. Brink, B. J. Kooi, H. J. Heeres and I. Melián-Cabrera, *Chem. Mater.*, 2013, **25**, 848.

16 X. Jiang, H. Oveisi, Y. Nemoto, N. Suzuki, K. C. W. Wu and Y. Yamauchi, *Dalton Trans.*, 2011, **40**, 10851.

17 S. M. Grant, A. Vinu, S. Pikus and M. Jaroniec, *Colloids Surf., A*, 2011, **385**, 121.

18 Q. Wu, F. Zhang, J. Yang, Q. Li, B. Tu and D. Zhao, *Microporous Mesoporous Mater.*, 2011, **143**, 406.

19 J. Fan, S. W. Boettcher and G. D. Stucky, *Chem. Mater.*, 2006, **18**, 6391.

20 X. Yuan, S. Xu, J. Lü, X. Yan, L. Hu and Q. Xue, *Microporous Mesoporous Mater.*, 2011, **138**, 40.

21 S. M. Morris, P. F. Fulvio and M. Jaroniec, *J. Am. Chem. Soc.*, 2008, **130**, 15210.

22 L. Xu, H. Song and L. Chou, *Int. J. Hydrogen Energy*, 2013, **38**, 7307

23 L. Xu, H. Song and L. Chou, *ACS Catal.*, 2012, **2**, 1331.

24 X. Wang, D. Pan, M. Guo, M. He, P. Niu and R. Li, *Mater. Lett.*, 2013, **97**, 27.

25 F. Huang, Y. Zheng, Z. Li, Y. Xiao, Y. Zheng, G. Cai and K. Wei, *Chem. Comm.*, 2011, **47**, 5247.

26 Q. Sun, Y. Zheng, Y. Zheng, Y. Xiao, G. Cai and K. Wei, *Scripta Mater.*, 2011, **65**, 1026.

27 Q. Sun, Y. Zheng, Z. Li, Y. Zheng, Y. Xiao, G. Cai and K. Wei, *Phys. Chem. Chem. Phys.*, 2013, **15**, 5670.

28 T. Horiuchi, T. Osaki, T. Sugiyama, K. Suzuki and T. Mori, *J. Non-Cryst. Solids*, 2001, **291**, 187.

29 X. Wang, Y. Guo, G. Lu, Y. Hu, L. Jiang, Y. Guo and Z. Zhang, *Catal. Today*, 2007, **126**, 369.

30 T. Horiuchi, L. Chen, T. Osaki, T. Sugiyama, K. Suzuki and T. Mori, *Catal. Lett.*, 1999, **58**, 89.

31 X. Guo, W. Li, K. Nakanishi, K. Kanamori, Y. Zhu and H. Yang, *J. Eur. Ceram. Soc.*, 2013, **33**, 1967-1974.

32 A. Mitra, D. Jana and G. De, *Microporous Mesoporous Mater.*, 2012, **158**, 187.

33 W. Cai, J. Yu, C. Anand, A. Vinu and M. Jaroniec, *Chem. Mater.*, 2011, **23**, 1147.

34 X. Shang, X. Wang, W. Nie, X. Guo, X. Zou, W. Ding and X. Lu, *J. Mater. Chem.*, 2012, **22**, 23806.

35 Y. Wang, W. Li, X. Jiao and D. Chen, *J. Mater. Chem. A*, 2013, **1**, 10720.

36 S. Hartmann, A. Sachse and A. Galarneau, *Materials*, 2012, **5**, 336.

37 J. Parmentier and S. Vilminot, *Chem. Mater.*, 1997, **9**, 1134.

38 C. Gerardin, S. Sundaresan, J. Benziger and A. Navrotsky, *Chem. Mater.*, 1994, **6**, 160.

39 H. Arai and M. Machida, *Appl. Catal., A*, 1996, **138**, 161.

40 D. A. Ward and E. I. Ko, *Chem. Mater.*, 1993, **5**, 956.

41 X. Chen and L. Gu, *J. Mater. Process. Technol.*, 2009, **209**, 3991.

42 Z. Li, F. Shi, L. Li, T. Zhang and C. Yan. *Phys. Chem. Chem. Phys.*, 20113, **13**, 2488.

43 E. Paparazzo, *Surf. Interface Anal.*, 1988, **12**, 115.

44 S. Thomas and P. M. A. Sherwood, *Anal. Chem.*, 1992, **64**, 2488.

45 E. Hoque, J. A. DeRose, P. Hoffmann, B. Bhushan and H. J. Mathieu, *J. Phys. Chem. C*, 2007, **111**, 3956.

46 H. He, K. Alberti, T. L. Barr and J. Klinowski, *J. Phys. Chem.*, 1993, **97**, 13703.

47 L.-H. Song and S. B. Park, *J. Nanosci. Nanotechnol.*, 2010, **10**, 122.

48 T. M. B. Campos, L. S. Cividanes, D. D. Brunelli, K. K. Sakane and G. P. Thim, *J.Eur. Ceram. Soc.*, 2012, **32**, 835.